


Article

Structure and Raman Spectra of C_{60} and C_{70} Fullerenes Encased into Single-Walled Boron Nitride Nanotubes: A Theoretical Study

Brahim Fakrach ¹, Fatima Fergani ¹, Mourad Boutahir ¹, Abdelhai Rahmani ¹ ,
Hassane Chadli ^{1,2}, Patrick Hermet ³ and Abdelali Rahmani ^{1,*}

¹ Laboratoire d'Etude des Matériaux Avancés et Applications (LEM2A), Université Moulay Ismaïl, FSM-ESTK-ESTM, BP 11201, Zitoune, 50000 Meknes, Morocco; fakrach@gmail.com (B.F.); fati.fergani@gmail.com (F.F.); mourad.boutahir@gmail.com (M.B.); rahmani614@gmail.com (A.R.); h.chadli@fpe.umi.ac.ma (H.C.)

² Equipe Physique Informatique et Modélisation des Procédés, Ecole Supérieur de Technologie BP 170, 54000 Khénifra, Morocco

³ Institut Charles Gerhardt Montpellier, UMR-5253, CNRS, Université de Montpellier, ENSCM, Place E. Bataillon, 34095 Montpellier, France; patrick.hermet@unmontpellier.fr

* Correspondence: a.rahmani@fs-umi.ac.ma

Received: 26 January 2018; Accepted: 27 February 2018; Published: 3 March 2018

Abstract: We report the structures and the nonresonant Raman spectra of hybrid systems composed of carbon fullerenes (C_{60} and C_{70}) encased within single walled boron nitride nanotube. The optimal structure of these systems are derived from total energy minimization using a convenient Lennard-Jones expression of the van der Waals intermolecular potential. The Raman spectra have been calculated as a function of nanotube diameter and fullerene concentration using the bond polarizability model combined with the spectral moment method. These results should be useful for the interpretation of the experimental Raman spectra of boron nitride nanotubes encasing C_{60} and C_{70} fullerenes.

Keywords: BN nanotube; fullerene; peapod; Raman spectroscopy; spectral moment's method; structure

1. Introduction

The discovery of nanomaterials such as fullerenes [1], carbon nanotubes [2] and boron nitride nanotubes [3] prevails over science and technology at nanoscale levels and becomes a hot topic for researchers and industrialists. Single walled carbon nanotubes (SWCNTs) filled with C_{60} fullerenes are commonly called carbon peapods ($C_{60}@SWCNT$). They have been firstly synthesized by Smith et al. in 1998 [4] and exhibit special physical properties with different potential applications [5–11].

Similar to SWCNTs, single walled boron nitride nanotubes (SWBNNTs) can also be filled with fullerene molecules such as C_{60} and C_{70} : they are so-called boron nitride peapods ($C_n@SWBNNT$ where $n = 60$ or 70). The $C_{60}@SWBNNT$ system was first theoretically proposed by Okada et al. [12] and experimentally synthesized two years later [13,14]. This system has aroused great interest in BN peapods as an ideal model to study the atoms or molecules in 1D confined conditions [13,15]. Due to its unusual electronic structure, the $C_{60}@SWBNNT$ is an interesting candidate to study a possible superconducting state.

It was theoretically stated [15–17] that (i) C_{60} inside SWBNNT is energetically more stable and achieved faster than C_{60} inside SWCNT and (ii) the suction force on the C_{60} induced by SWBNNTs is higher than that induced by the SWCNTs [12,16]. The C_{60} - C_{60} intermolecular distance inside the SWBNNT is 0.9 nm [13,18], which is slightly smaller than the 1.0 nm intermolecular distance for

carbon peapods [5,19]. This difference could be due to a stronger van der Waals attraction between the SWBNNT and the C_{60} or possibly to commensurability effects [13,18]. Moon et al. [20] have demonstrated from molecular dynamics simulation that the (10,10) and (17, 0) SWBNNTs are the most favorable for encapsulation of C_{60} molecules. Mickelson et al. [13] have shown that the C_{60} 's structure inside SWBNNTs is dependent of the tube diameter, as in the case of C_{60} @SWCNT [21–24]. Compared to other nanostructures, nanopeapods have opened new applications such as storage materials with high capacity and stability [10,25] and considered to be potential materials for high-temperature superconductors [11]. The space inside the nanotube can be also regarded as a nanometer-sized container for chemical reactions [7].

Raman spectroscopy is the standard characterization technique for nanotubes. Raman spectrum of C_{60} @SWBNNT have been reported in the literature at different laser energies (488, 568 and 647 nm) [14]. All fundamental Raman lines of the encapsulated C_{60} peas are observed and a structured peak at 268, 330, 355 and 466 cm^{-1} is measured and assigned to the reaction products of the carbon fullerenes inside the BN nanotubes. The authors show that the radial breathing mode range reveals new spectral features which are not observed in the case of unfilled BN tubes.

The experimental Raman spectra measured on BN peapods are complex to analyze because experiments performed on macroscopic samples consist of a mixture of bundles of tubes of different diameters and chiralities. In this paper, in order to improve the comparison between the calculations and experimental data, we investigate theoretically the fullerene-fullerene and fullerene-tube interactions effect on the vibrations of C_{60} and C_{70} BN peapods. In contrast with C_{60} molecules, the ellipsoidal shape of C_{70} leads both the C_{70} - C_{70} and C_{70} -SWBNNT interactions to be anisotropic. As a consequence, the electronic structure and the ground state energy of fullerene peapods depend on the configuration of the fullerene molecules inside the nanotubes. The analysis of the Raman spectra of peapods suggests that the observed shifts of the radial breathing mode (RBM) could be explained by a small increase of the tube diameter, resulting from the interaction between π -electrons of the fullerene with the interior of the nanotube [26].

In previous works [23,27,28], we studied the different possible configurations of C_{60} and C_{70} molecules encapsulated into SWCNTs with diameter lower than 2.28 nm. Raman spectra of C_{60} carbon peapods have been calculated for C_{60} linear, zigzag, double helix and layer of two molecules configurations within the bond-polarizability model. Our results were in qualitative agreement with the experimental ones. Here, we continue these studies in the case where the C_{60} and C_{70} molecules are now encapsulated into SWBNNTs. Our work addresses new questions as to the influence of the nanotube diameter and the C_{60} and C_{70} filling rate. In this context, we use a direct diagonalization of the dynamical matrix for small peapods (few hundred atoms) and the spectral moment method for larger ones. We report the structural organization of the C_{60} @SWBNNT and C_{70} @SWBNNT as a function of the diameter and the chirality of the BN nanotubes and we discuss the change in the Raman response of these hybrid systems including the influence of the fullerene concentration.

2. Models and Simulation Method

2.1. Structure and Dynamics of C_{60} @SWBNNT and C_{70} @SWBNNT Peapods

SWBNNTs are obtained by rolling a single hexagonal boron nitride sheet [29,30] and can be specified by integers (n, m) which define the translation vector between two equivalent points. A BN peapod consists of fullerene molecules trapped inside a SWBNNT host. Depending on the nanotube diameter, different configurations of C_{60} and C_{70} can certainly exist. Here, we restrict our study by considering only a linear chain of C_{60} and C_{70} confined inside SWBNNT. Considering a (10,10) SWBNNT, Figure 1 shows the structures of the encapsulated C_{60} and C_{70} . The configuration of the guest C_{60} and C_{70} molecules inside SWBNNTs is derived from total energy minimizations according to the procedure described in our previous works on carbon peapods [23].

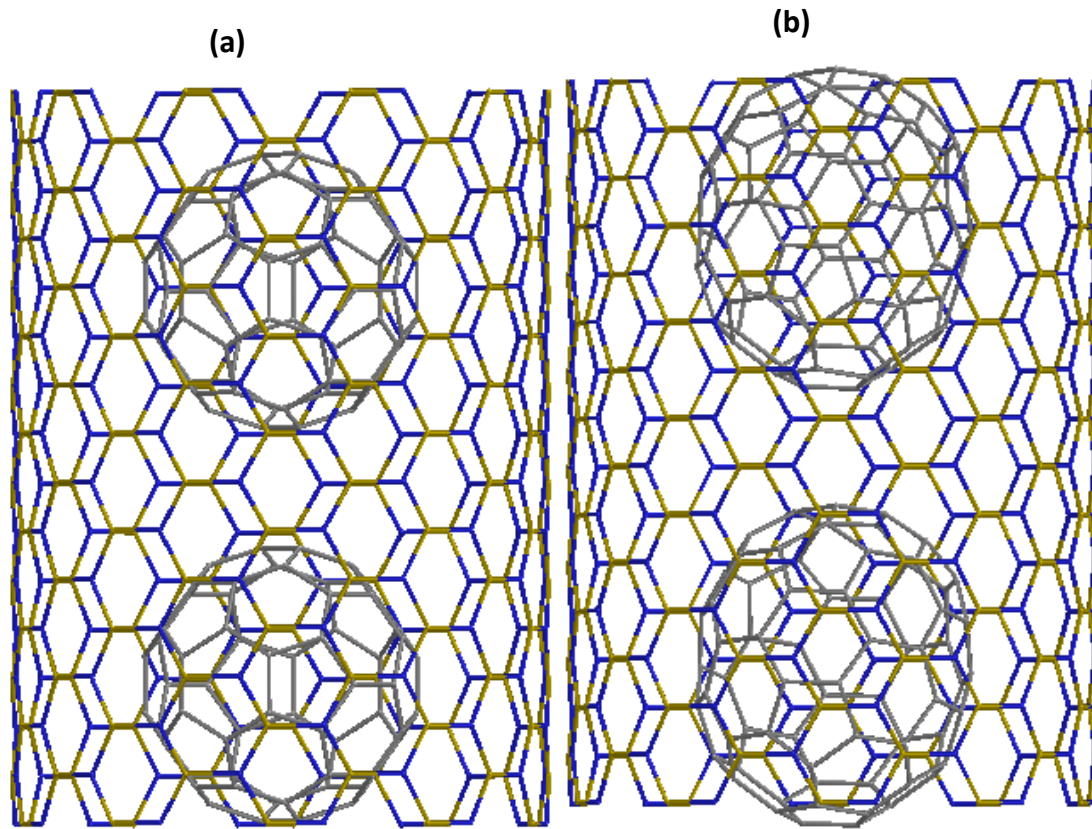


Figure 1. Structure of two SWBNNT peapods: (a) C₆₀@(10,10) and (b) C₇₀@(10,10).

The C-C interaction between carbon atoms belonging to non-bonded fullerenes, and between fullerenes and the surrounding nanotube, are represented by the Lennard-Jones potential, $U_{LJ}(r) = 4\epsilon \left[\left(\frac{\sigma}{r} \right)^{12} - \left(\frac{\sigma}{r} \right)^6 \right]$. For boron, nitrogen and carbon atoms, the ϵ_{ii} -parameter is 0.004116, 0.006281 and 0.002635 eV, whereas the σ_{ii} -parameter is 0.3453, 0.3365 and 0.3369 nm, respectively [16,31]. The parameters ϵ_{ij} and σ_{ij} between different atoms are calculated by the following Lorentz-Berthelot rules: $\epsilon_{ij} = \sqrt{\epsilon_i \epsilon_j}$ and $\sigma_{ij} = (\sigma_i + \sigma_j) / 2$.

The intratube interactions at the surface of the SWBNNT are described by the same force constant model we recently used in the calculations of the infrared spectra of single walled boron nitride nanotubes [32]. The C-C intramolecular interactions between carbon atoms at the surface of C₆₀ molecules are modeled by the force constants model described by Jishi and Dresselhaus [33]. Interactions up to the fourth nearest neighbors are accounted to derive the dynamical matrix. The dynamical matrix of free C₇₀ molecule was calculated using the density functional theory (DFT) as implemented inside the SIESTA package [34]. The dynamical matrix (leading to the frequency of the Raman lines) is calculated by block using the previous intramolecular potentials and van der Waals potential (i.e., fullerene-SWBNNT and fullerene-fullerene interactions).

2.2. Methods

The time-averaged power flux of the Raman scattered light in a given direction, with a frequency between ω_d and $\omega_d + d\omega_d$ within a solid angle $d\Omega$, is related to the differential scattering cross section:

$$\frac{d^2 S}{d\Omega d\omega_d} = \frac{\omega_d^4}{16\pi^2 c^4} [B(\omega) + 1] \hbar \sum_{ijkl} v_i v_k I_{ijkl}(\omega) w_j w_l \quad (1)$$

where

$$I_{ijkl}(\omega) = \sum_m a_{ij}^*(m) a_{kl}(m) \frac{1}{2\omega_m} [\delta(\omega - \omega_m) - \delta(\omega + \omega_m)] \quad (2)$$

and $\omega = \omega_0 - \omega_d$ is the Raman shift. In these equations, (i,j,k,l) -indices denote the Cartesian components, the star symbolizes the complex conjugation, c is the speed of light in the medium, \hbar is the reduced Planck constant, ω_0 (resp. ω_d) is the frequency of incident (resp. scattered) light, v (resp. w) is the polarization unit vector of the incident (resp. scattered) light, $B(\omega)$ is the Bose factor, and ω_m is the frequency of the m th zone-center phonon mode. The Raman susceptibility tensor is defined as,

$$a_{ij}(m) = \sqrt{\Omega_0} \sum_{\kappa\gamma} \pi_{ij,\gamma}^{\kappa} u_m(\kappa\gamma) \quad (3)$$

where the sum runs over all atoms κ and space directions γ , Ω_0 is the unit cell volume, $u_m(\kappa\gamma)$ is the $(\kappa\gamma)$ component of the m th phonon eigendisplacement vector, and $\tilde{\pi}$ is a third-rank tensor describing the changes of the first-order optical dielectric susceptibility ($\tilde{\chi}^\infty$) induced by individual atomic displacements. This latter quantity is defined as,

$$\pi_{ij,\gamma}^{\kappa} = \frac{\partial \chi_{ij}^\infty}{\partial \tau_{\kappa\gamma}} \quad (4)$$

where $\tau_{\kappa\gamma}$ corresponds to the displacement of the κ^{th} atom in the direction γ . As long as the phonon frequencies and eigendisplacements are known, $\tilde{\pi}$ is the central quantity to be determined to estimate Raman intensities. The first term of Equation (2), associated with the creation of a vibrational quantum, describes the Stokes scattering with a downshift in frequency ($\omega > 0$). The second term, related to an annihilation of a vibrational quantum, describes the anti-Stokes scattering with an upshift frequency ($\omega < 0$). The m th mode is Raman active if one component of the Raman susceptibility tensor, $a_{ij}(m)$, is nonnull.

The Raman intensities can be calculated within the framework of the nonresonant bond polarizability model [35]. In this model, we consider that the optical dielectric susceptibility ($\tilde{\chi}^\infty$) of the crystal can be decomposed into individual contributions, arising only from the polarizability ($\tilde{\alpha}^b$) of bonds b between nearest-neighbor atoms,

$$\chi_{ij}^\infty = \frac{1}{\Omega_0} \sum_b \alpha_{ij}^b \quad (5)$$

and the polarizability of a particular bond b is assumed to be given by the empirical equation:

$$\alpha_{ij}^b = \frac{1}{3}(\alpha_l + 2\alpha_p)\delta_{ij} + (\alpha_l - \alpha_p)(\hat{r}_i\hat{r}_j - \frac{1}{3}\delta_{ij}) \quad (6)$$

where \hat{r} is the unit vector along the bond b . The parameters α_l and α_p correspond to the longitudinal and perpendicular bond polarizability, respectively. A further assumption is that the parameters of this model are functions of the bond lengths r only, so that the derivative of the polarizability tensor with respect to the displacement of atom κ in direction γ is given by:

$$\frac{\partial \alpha_{ij}^b}{\partial \tau_{\kappa\gamma}} = \frac{1}{3}(2\alpha'_p + \alpha'_l)\delta_{ij}\hat{r}_\gamma + (\alpha'_l - \alpha'_p)(\hat{r}_i\hat{r}_j - \frac{1}{3}\delta_{ij})\hat{r}_\gamma + \frac{\alpha_l - \alpha_p}{r}(\delta_{i\gamma}\hat{r}_j + \delta_{j\gamma}\hat{r}_i - 2\hat{r}_i\hat{r}_j\hat{r}_\gamma) \quad (7)$$

where $\alpha'_l = (\frac{\partial \alpha_l}{\partial r})_{r=r_0}$, $\alpha'_p = (\frac{\partial \alpha_p}{\partial r})_{r=r_0}$ and r_0 is the equilibrium bond distance. The values of these α' -parameters are usually fitted with respect to the experiments [35].

Raman spectra are calculated using a direct diagonalization of the dynamical matrix for small samples (few hundreds atoms). When the system contains a large number of atoms, the dynamical matrix is very large and its diagonalization fails or requires long computing time. In contrast,

the spectral moments method allows to compute directly the Raman spectrum of very large harmonic systems without any diagonalization of the dynamical matrix [36–39].

In all our calculations, the nanotube axis is along the Z-axis and a carbon atom is along the X-axis of the nanotube reference frame. The laser beam is kept along the Y-axis of the reference frame. We consider that both incident and scattered polarizations are along the Z-axis to calculate the ZZ-polarized spectra.

3. Results and Discussion

3.1. Optimized Structure of C_{60} @SWBNNT and C_{70} @SWBNNT

The optimal configuration of the inserted fullerene molecules inside the tube is calculated by minimizing the energy of the C_{60} –SWBNNT and C_{60} – C_{60} interactions described by the Lennard-Jones potential. Results are listed in Table 1 for tubes whose diameter is between 1.30 and 1.45 nm. The linear chain is the optimal configuration for the tubes having a diameter $D_{tube} = 2(R + d)$, where R is the C_{60} fullerene radius and d is the interlayer C_{60} –SWBNNT distance. The optimal C_{60} – C_{60} gap inside SWBNNTs is calculated around 1.0 ± 0.05 nm for all optimized peapods. This value is larger than the one observed by Zettl et al. [18] (≈ 0.89 nm). This difference could be due to a stronger van der Waals attraction between the nanotube and the C_{60} .

In contrast with C_{60} molecules, the ellipsoidal shape of C_{70} leads both the C_{70} – C_{70} and C_{70} –SWBNNT interactions to be anisotropic. In our calculations, we considered a number of C_{70} molecules initially placed such that their long axis was parallel to the nanotubes axis. The energy minimization of the different C_{70} @SWBNNTs is performed for any molecular orientation characterized by three Euler angles (following the terminology used by Bradley et al. [40]). Only the rotation angle $0 \leq \theta \leq 90^\circ$ over the tube-axis can vary during our structural relaxation procedures. Thus, the optimum C_{70} packing can be characterized by the degree of inclination θ : $\theta = 0^\circ$ for lying orientation, $\theta = 90^\circ$ for standing orientation and $0 < \theta < 90^\circ$ for tilted orientation. Our calculations show that this angle increases with the diameter of nanotubes (see Table 2) and no correlation is clearly observed between this angle and their chirality.

Both for the C_{60} @SWBNNTs and C_{70} @SWBNNTs, the interlayer C_{60} –SWBNNT and C_{70} –SWBNNT distance is between 0.301 and 0.351 nm (see Tables 1 and 2). These values are consistent with the experimental ones [41–46] and quite close to the interplanar distance in a bulk hexagonal-BN.

Table 1. Optimized structural parameters of the C_{60} molecules inside SWBNNT in diameter range where the C_{60} molecules adopt a linear chain inside nanotubes.

SWBNNT Index (n,m)	SWBNNT Diameter (nm)	SWBNNT Chirality (deg)	C_{60} –SWBNNT Distance (nm)	C_{60} – C_{60} Distance (nm)
(11,8)	1.307	24.80	0.303	1.010
(12,7)	1.316	21.36	0.307	1.007
(13,6)	1.330	18	0.314	1.007
(17,0)	1.344	0	0.321	1.010
(14,5)	1.351	14.70	0.324	1.000
(10,10)	1.370	30	0.334	1.008
(15,4)	1.372	11.52	0.335	1.010
(12,8)	1.379	23.41	0.339	1.009
(14,6)	1.406	17	0.351	1.009
(18,0)	1.424	0	0.350	1.003
(11,10)	1.439	28.42	0.349	1.005
(13,8)	1.452	22.17	0.334	1.012

Table 2. Optimized structural parameters of the C_{70} molecules inside BNNT in diameter range where the C_{70} molecules adopt a linear chain inside nanotubes.

SWBNNT Index (n,m)	SWBNNT Diameter (nm)	SWBNNT Chirality (deg)	C_{70} -SWBNNT Distance (nm)	Angle θ (deg)	C_{70} - C_{70} Distance (nm)
(13,6)	1.330	18	0.307	0	1.1273
(17,0)	1.344	0	0.314	0	1.1276
(14,5)	1.351	14.70	0.317	0	1.1280
(10,10)	1.370	30	0.327	0	1.1281
(15,4)	1.372	11.52	0.3028	0	1.1280
(14,6)	1.406	17	0.305	2	1.1260
(18,0)	1.424	0	0.309	40	1.1079
(11,10)	1.439	28.42	0.301	47	1.1060
(18,1)	1.465	2.68	0.304	65	1.0821
(17,3)	1.478	8	0.325	90	1.0039

3.2. Raman Spectra of Completely Filled Peapods

We study the Raman active modes in C_{60} @SWBNNTs and C_{70} @SWBNNTs. For this purpose, a peapod filled to saturation has been considered. The calculated ZZ-polarized Raman spectra of C_{60} @(10,10) and C_{70} @(10,10), with their corresponding unfilled (10,10) armchair SWBNNT (tube diameter close of 1.37 nm), and the unoriented C_{60} and C_{70} molecules are displayed in Figure 2. Raman lines can be divided into three frequency ranges: (i) below 200 cm^{-1} where the breathing-like modes (BLM) dominate, (ii) an intermediate range between 200 and 600 cm^{-1} , and (iii) above 1350 cm^{-1} where the tangential-like modes (TLM) are located. Infinite peapods have been obtained by applying periodic conditions along the tube axis.

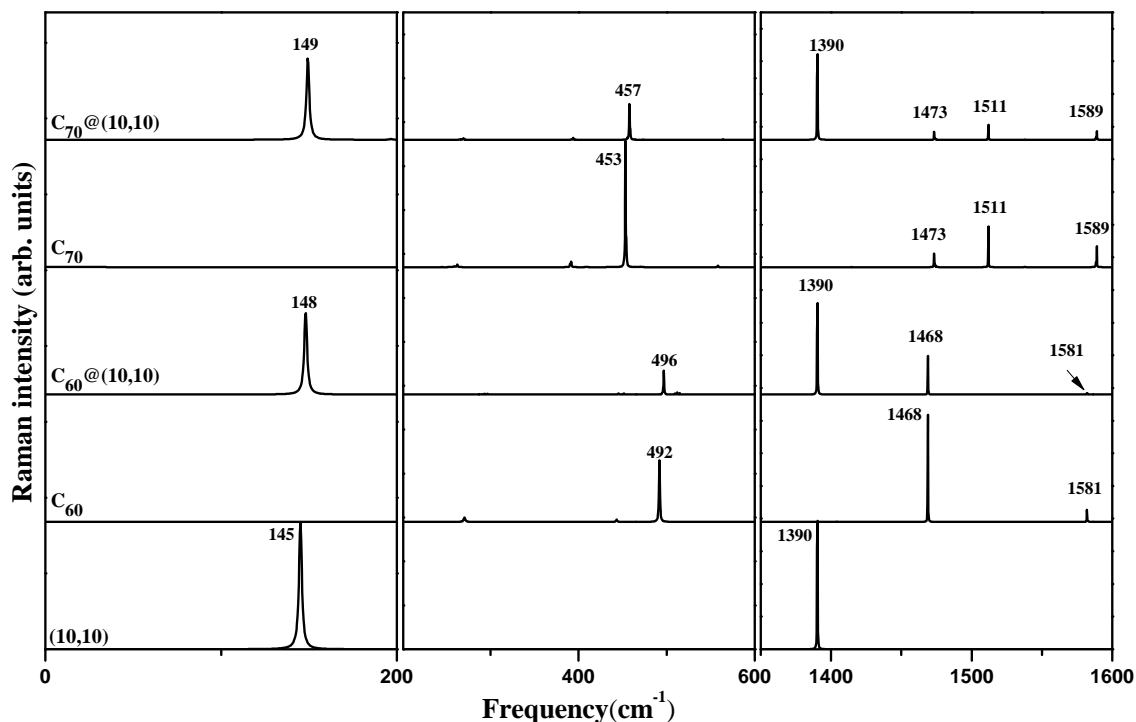


Figure 2. Calculated ZZ-polarized Raman spectra of infinite C_{60} @(10,10) and C_{70} @(10,10) peapods. Spectra of infinite empty (10,10) SWBNNT, C_{60} and C_{70} molecules are also reported for references.

The main modes of the (10,10) SWBNNT, and the C_{60} and C_{70} molecules, are almost not affected by the encapsulation in the TLM region. Indeed, in this region, the position and the relative intensity of the Raman lines observed in peapods is a superposition of the Raman lines of each of the sub-systems. For the BLM region, an upshift of the RBM of the tube is observed when the C_{60} and C_{70} molecules are encapsulated into the tube. For instance, the RBM of the unfilled (10,10) SWBNNT shifts from 145 cm^{-1} in empty (10,10) to 148 and 149 cm^{-1} in completely filled $C_{60}@ (10,10)$ and $C_{70}@ (10,10)$, respectively. In the two kinds of peapods, these modes are assigned to the radial breathing like mode (RBLM) of the tube where all atoms in the tube and in the surface of fullerene adjacent to the tube move in phase along the radial direction (see Figure 3a,b). In contrast, the atoms in adjacent surfaces of fullerenes move in counter-phase along the axial direction. In the intermediate range between 200 and 600 cm^{-1} , only phonon modes of the C_{60} and C_{70} molecules can be observed. The line centered at 492 cm^{-1} and assigned as the symmetric A_g mode of C_{60} shifts to 496 cm^{-1} in $C_{60}@ (10,10)$ peapod. Similarly, the line centered at 453 cm^{-1} in C_{70} and assigned as the symmetric A'_1 mode shifts to 457 cm^{-1} with the encapsulation. These calculated upshifts can be explained by the van der Waal intermolecular interactions acting between the fullerenes and the SWBNNTs. Concerning the atomic motions modified by the encapsulation, we displayed in Figure 3, the eigendisplacement vectors of these two Raman modes obtained in peapods (Figure 3f,g) from the direct diagonalization of the dynamical matrix, together with the RBM of the unfilled (10,10) SWBNNTs (Figure 3d) and the pure C_{60} (Figure 3c) and C_{70} (Figure 3e) molecules. We observe in peapods, a counter-phase coupled motion of the breathing modes of the encapsulated molecule and the tube, and all atoms of the C_{60} and C_{70} molecules vibrate in-phase in the radial direction (see Figure 3f,g).

In the remainder of this paper, we focus on the low frequency range of the ZZ-polarized Raman spectrum of BN peapods. We investigated the dependence of some specific Raman active modes of infinite peapods as a function of the diameter of the nanotube. We already reported that the RBM is the most influenced mode by the nanotube filling. This mode is also the most appropriate for extracting structural and dynamical information of SWBNNT. A few years ago, we found [32,47], using the bond polarizability model combined with the spectral moments method, a relation for isolated tubes between their diameter D and their RBM frequency: $\omega_{RBM} = a/D$, where $a = 198\text{ nm.cm}^{-1}$. This relation was in agreement with the different approaches reported in the literature [48–50]. Figure 4 shows the RBM frequency in SWBNNTs and the RBLM frequency in $C_{60}@ \text{SWBNNTs}$ and $C_{70}@ \text{SWBNNTs}$ as a function of the inverse tube diameter. For the two kinds of peapods, the evolution of the RBLMs is qualitatively the same as those of the RBM: their frequencies decrease when the tube diameters increase. However, the RBLMs show deviation from the scaling law stated for the RBM frequency and this deviation is even more important when the diameter of the tubes is small (below 1.35 nm). Both for the C_{60} peapods and C_{70} peapods, we found that the frequency of the RBLM follows a law in $a/D + b$ with $a = 363.6\text{ nm.cm}^{-1}$ and $b = -116.7\text{ cm}^{-1}$ for C_{60} peapods and $a = 320.9\text{ nm.cm}^{-1}$ and $b = -85\text{ cm}^{-1}$ for C_{70} peapods.

3.3. Raman Spectra of Incompletely Filled Peapods

In real peapod samples, it is reasonable to consider that all the nanotubes are not completely filled with C_{60} or C_{70} and the highest filling rates range from 70 to 90% [51,52]. The exact degrees of filling is still under discussion and ranges from a certain percent to almost 100% filling. In this section, we make the hypothesis of partial filling of the tubes with a quasi infinite long chain. This hypothesis is supported by observations reported in Ref. [53]. Very long tubes are considered (more than 100 cells) and a defined number of molecules C_{60} and C_{70} are inserted. To avoid finite size effects, we applied periodic conditions along the tube axis.

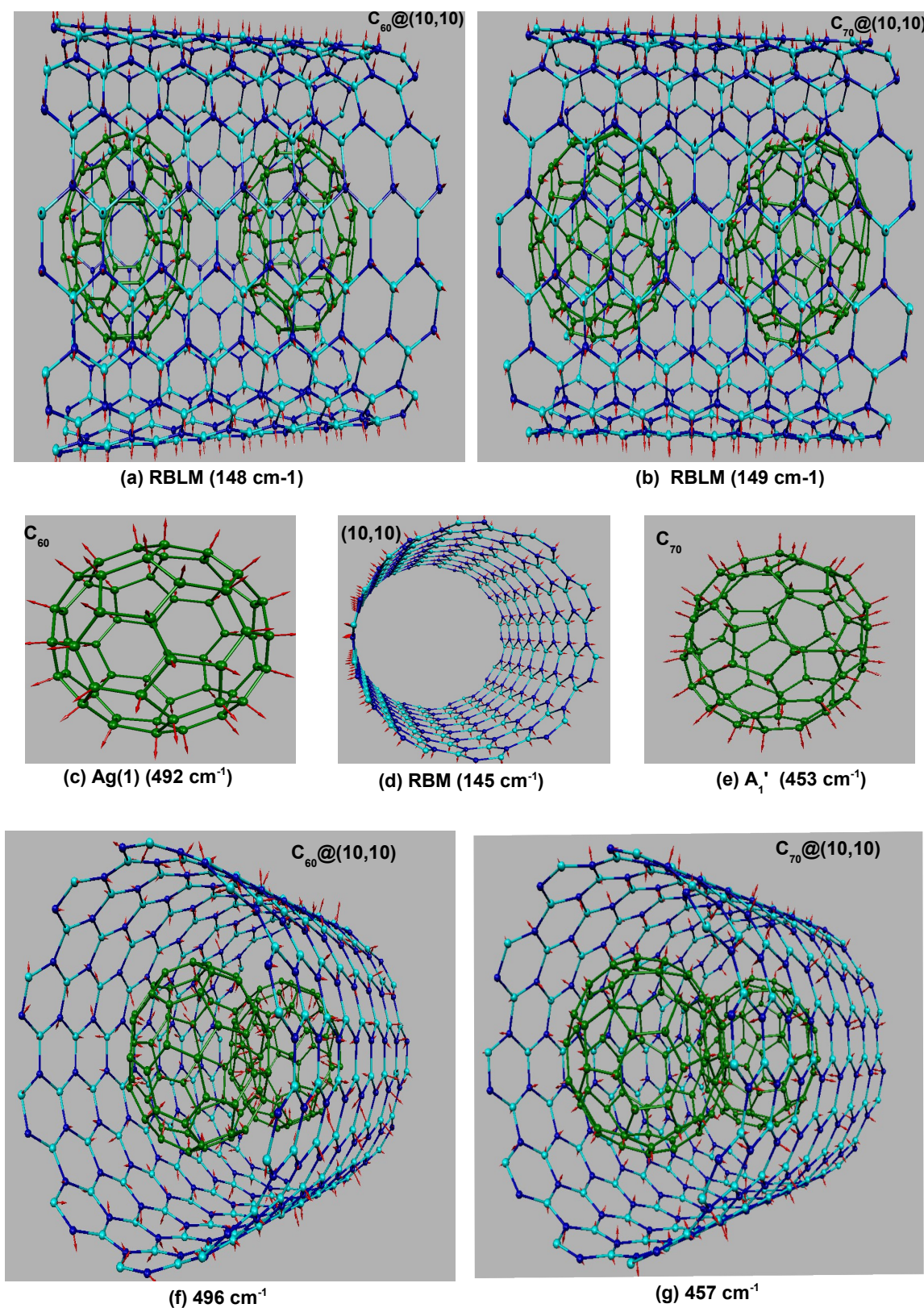


Figure 3. Calculated atomic motions (eigendisplacement vectors) in C₆₀, C₇₀, (10,10) SWBNNT, C₆₀@(10,10) and C₇₀@(10,10). Arrows are proportional to the amplitude of the atomic motions.

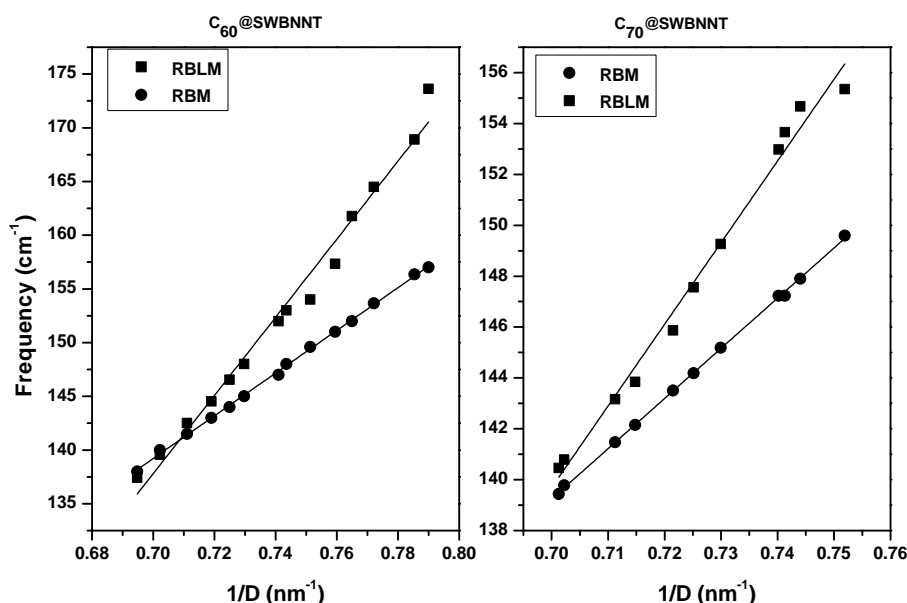


Figure 4. Calculated RBLM frequencies (squares) in isolated infinite nanopeapods and RBM (circles) frequencies in infinite isolated SWBNNTs. Only tubes with a diameter below 1.42 and 1.45 nm are considered for C₆₀@SWBNNT and C₇₀@SWBNNT, respectively.

We found that the number of molecules inside the SWBNNT has no significant effect on the Raman spectrum except on the RBLM mode which is the most sensitive to the degree of filling of the SWBNNTs. Figure 5 displays the ZZ-polarized Raman spectra below 600 cm⁻¹ of C₆₀@(10,10) and C₇₀@(10,10) linear peapods as a function of their filling rate. Five values of the filling rate have been considered: $F = 20, 40, 60, 80$ and 100% corresponding to 2, 4, 8, 12 and 16 encapsulated molecules (C₆₀ or C₇₀). We observe that all Raman lines undergo a frequency upshift more or less significant as the filling level increases. Similarly, the intensity of the C₆₀ and C₇₀ characteristic lines increases. A single RBLM peak characterizes all spectra for $F = 20$ and 100% of the filling factor. For $F = 100\%$ (tubes completely filled) the RBLM peak is located at 148 and 149 for C₆₀@(10,10) and C₇₀@(10,10) respectively and at 145 for $F = 20\%$ (low filling level). Let us call ω_h and ω_l the frequency of the heavy and light filling factor, the increase of F from 20 to 100% leads to the appearance of two peaks at frequency close to ω_h and ω_l . The intensity of these peaks shifts from the one located around ω_l to that located around ω_h when increasing F . This last behaviour is observed for carbon peapods [54].

The lines at 291, 496 and 510 cm⁻¹ respectively upshifts to 296, 497 and 512 cm⁻¹ and increases in intensity from 20 to 100% for C₆₀@(10,10). The same the lines centered at 266, 493 and 457 cm⁻¹ increases in intensity from 20 to 100% for C₇₀@(10,10). The observed frequency shift can be associated with C₆₀-SWBNNT, C₇₀-SBNN, C₆₀-C₆₀ and C₇₀-C₇₀ van der Waals interaction effects.

Using the spectral moment's method, we investigate the evolution of the average nonresonant intensity ratios between Raman mode of C₆₀ molecules and BN nanotube as a function of the concentration of C₆₀s inside the tubes. In the case of C₆₀ carbon peapods, we have found that the dependence of the Raman spectrum with the filling factor, the relative intensity ratio between a Raman mode of C₆₀ and a mode of SWBNNT, normalized by the same ratio calculated for a reference filling factor, gives a useful method to derive from Raman experiments the relative concentration of C₆₀ in peapods samples prepared with the same batch as that of the reference filling factor sample.

First, we calculate the Raman spectrum at different filling factors and for each filling factor. Then, for each filling factor, the integrated intensity ratios between Raman mode of C₆₀ molecules and the RBLM (for C₆₀ phonon modes: Hg(2), Ag(1), Hg(3) and Hg(4)) or G-mode (for C₆₀ phonon modes: Hg(7) and Ag(2)) are calculated. These calculated intensity ratios are normalized with respect to the same intensity ratios calculated for the 60% filling factor sample. The obtained relative

concentrations derived by this way in the case $C_{60}@ (10,10)$ are shown in Figure 6. As expected, the relative concentrations calculated for each C_{60} mode are close especially for low frequency modes expect the Hg(7) and Ag(2) high frequency modes that could showing a overestimated concentration.

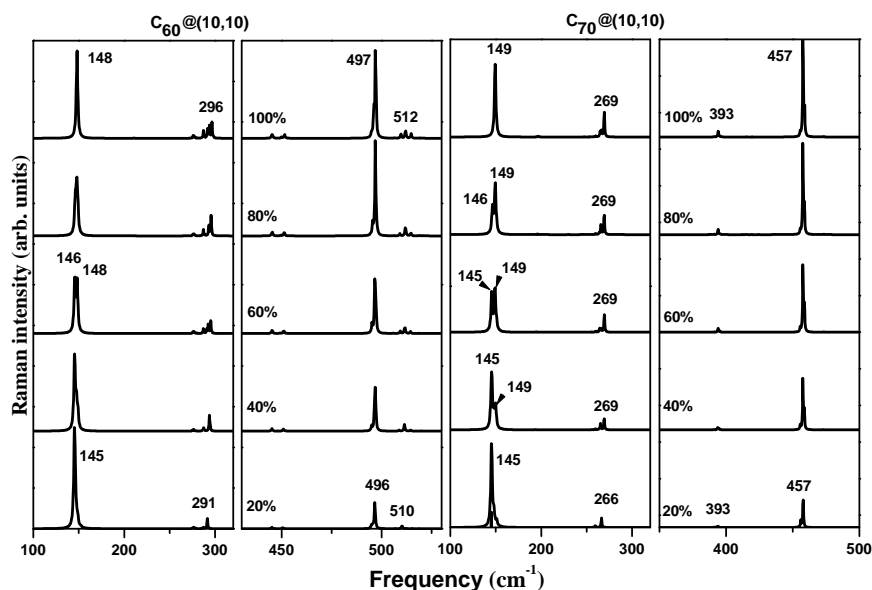


Figure 5. ZZ-polarized Raman spectra in RBLM regions for infinite nanopeapods as a function of their filling rate: $C_{60}@ (10,10)$ (left) and $C_{70}@ (10,10)$ (right).

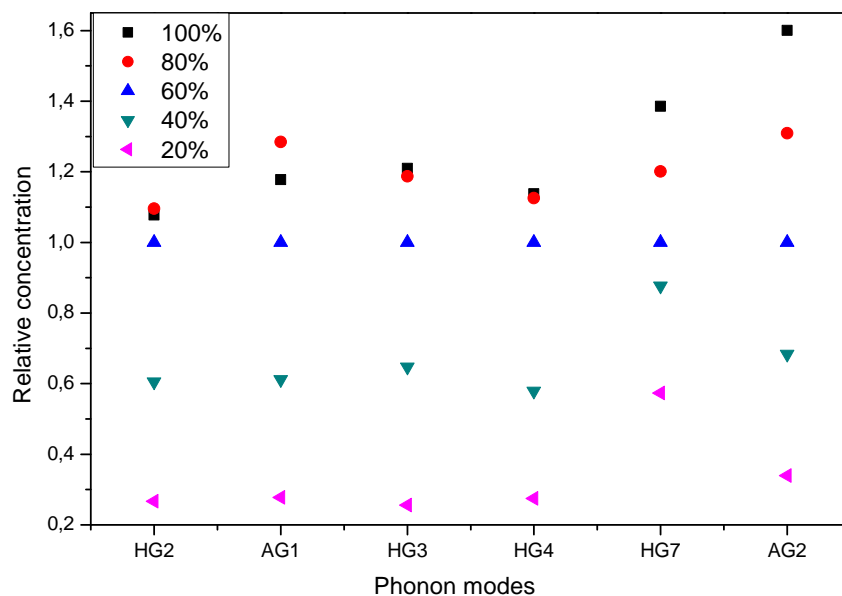


Figure 6. Calculated average intensity ratios, normalized on the 60% filling factor intensities, between modes of the C_{60} in the $C_{60}@ (10,10)$ peapod crystal and the RBLM (Hg(2), Ag(1), Hg(3), Hg(4)) or G-mode (Ag(2)) of the (10,10) BN nanotube.

4. Conclusions

We have calculated the nonresonant Raman spectrum of isolated boron nitride peapods. The C_{60} and C_{70} molecules adopt a linear arrangement for SWBNNTs diameter lower than 1.45 and 1.42 nm, respectively. Both for the obtained C_{60} and C_{70} peapods, the dependence of the Raman spectrum as a

function of the tube diameter and the filling rate have been analyzed. We showed that the configuration of the C_{60} and C_{70} molecules significantly impact the Raman line frequency as well as their intensities in the BN peapod structure. In particular, the line position is modulated by both fullerene-fullerene and fullerene-SWBNNT interactions, whereas the angle dependence of C_{70} 's affects their intensities in polarized spectra. We found that the behaviour of the RBLM mode with the pod diameter was clearly modified in peapod. This involves that the linear relation linking the RBLM frequency and the inverse of the tube diameter found in SWBNNT has to be modified in the case of peapod sample. We discussed the Raman signatures of the C_{60} and C_{70} peapods according to their filling rate and for the RBLM in particular. The relative intensity ratio between a Raman mode of C_{60} and C_{70} and a mode of SWBNNT, normalized by the same ratio calculated for a reference filling factor, could be a useful method to derive from Raman experiments the relative concentration of fullerenes in peapods samples prepared with the same batch as the reference filling factor sample. Finally, we think that the calculated Raman spectra reported in the present work can be useful to understand future Raman data.

Acknowledgments: The work was supported by the CNRS-France/CNRST-Morocco agreement.

Author Contributions: Brahim Fakrach, Fatima Fergani and Mourad Boutahir conceived and carried out the calculations. Abdelhai Rahmani and Hassane Chadli supervised the simulations and contributed to the text. Patrick Hermet and Abdelali Rahmani shared in the writing of the paper.

Conflicts of Interest: The authors declare no conflicts of interest.

References

1. Kroto, H.W.; Heath, J.R.; O'Brien, S.C.; Curl, R.F.; Smalley, R.E. C_{60} : Buckminsterfullerene. *Nature* **1995**, *318*, 162–163, doi:10.1038/318162a0.
2. Iijima, S. Helical microtubules of graphitic carbon. *Nature* **1991**, *354*, 56–58, doi:10.1038/354056a0.
3. Chopra, N.G.; Luyken, R.J.; Cherrey, K.; Crespi, V.H.; Cohen, M.L.; Louie, S.G.; Zettl, A. Boron nitride nanotubes. *Science* **1995**, *269*, 966–967, doi:10.1126/science.269.5226.966.
4. Smith, B.W.; Monthieux, M.; Luzzi, D. Encapsulated C_{60} in carbon nanotubes. *Nature* **1998**, *396*, 323–324, doi:10.1038/24521.
5. Smith, B.W.; Luzzi, D.E. Formation mechanism of fullerene peapods and coaxial tubes: A path to large scale synthesis. *Chem. Phys. Lett.* **2000**, *321*, 169–174, doi:10.1016/S0009-2614(00)00307-9.
6. Pluznick, J.L.; Zou, D.J.; Zhang, X.; Yan, Q.; Rodriguez-Gil, D.J.; Eisner, C.; Wells, E.; Greer, C.A.; Wang, T.; Firestein, S.; et al. Functional expression of the olfactory signaling system in the kidney. *Proc. Natl Acad. Sci. USA* **2009**, *106*, 2059–2064, doi:10.1073/pnas.0812859106.
7. Allen, C.S.; Ito, Y.; Robertson, A.W.; Shinohara, H.; Warner, J.H. Two-dimensional coalescence dynamics of encapsulated metallofullerenes in carbon nanotubes. *ACS Nano* **2011**, *5*, 10084, doi:10.1021/nn204003h.
8. Terrones, H. Beyond Carbon Nanopeapods. *ChemPhysChem* **2012**, *13*, 2273–2276, doi:10.1002/cphc.201200321.
9. Kwon, Y.K.; Tomanek, D.; Iijima, S. “Bucky Shuttle” memory device: Synthetic approach and molecular dynamics simulations. *Phys. Rev. Lett.* **1999**, *82*, 1470–1476, doi:10.1103/PhysRevLett.82.1470.
10. Cox, B.J.; Thamwattana, N.; Hill, J.M. Orientation of spheroidal fullerenes inside carbon nanotubes with potential applications as memory devices in nano-computing. *Physica A* **2008**, *41*, 235209, doi:10.1088/1751-8113/41/23/235209.
11. Service, R.F. Nanotube ‘Peapods’ Show Electrifying Promise. *Science* **2001**, *292*, 45, doi:10.1126/science.292.5514.45.
12. Okada, S.; Saito, S.; Oshiyama, A. Semiconducting form of the first-row elements: C_{60} chain encapsulated in BN nanotubes. *Phys. Rev. B* **2001**, *64*, 201303(R), doi:10.1103/PhysRevB.64.201303.
13. Mickelson, W.; Aloni, S.; Han, W.Q.; Cumings, J.; Zettl, A. Packing C_{60} in boron nitride nanotubes. *Science* **2003**, *300*, 467–469, doi:10.1126/science.1082346.
14. Hasi, F.; Simon, F.; Kuzmany, H.; Arenal De La Concha, R.; Loiseau, A. Raman spectroscopy of boron nitride nanotubes and boron nitride-Carbon composites. *AIP Conf. Proc.* **2005**, *786*, 340–344, doi:10.1063/1.2103883.
15. Thamwattana, N.; Hill, J.M. Continuum modelling for carbon and boron nitride nanostructures. *J. Phys. Condens. Matter* **2007**, *19*, 406209, doi:10.1088/0953-8984/19/40/406209.

16. Kang, J.W.; Hwang, H.J. Comparison of C60 encapsulations into carbon and boron nitride nanotubes. *J. Phys. Condens. Mat.* **2004**, *16*, 3901, doi:10.1088/0953-8984/16/23/010.
17. Trave, A.; Ribeiro, F.; Louie, S.; Cohen, M. Energetics and structural characterization of C60 polymerization in BN and carbon nanopeapods. *Phys. Rev. B* **2004**, *70*, 205418, doi:10.1103/PhysRevB.70.205418.
18. Zettl, A.; Cumings, J.; Weiqlang, H.; Mickelson, W. Boron nitride nanotube peapods. *AIP Conf. Proc.* **2002**, *633*, 140, doi:10.1063/1.1514092.
19. Burtiaux, B.; Claye, A.; Smith, B.W.; Monthieux, M.; Luzzi, D.E.; Fischer, J.E. Abundance of encapsulated C60 in single-wall carbon nanotubes. *Chem. Phys. Lett.* **1999**, *310*, 21–24, doi:10.1016/S0009-2614(99)00720-4.
20. Moon, W.H.; Son, M.S.; Lee, J.H.; Hwang, H.J. Molecular dynamics simulation of C60 encapsulated in boron nitride nanotubes. *Phys. Status Solidi B* **2004**, *241*, 1783, doi:10.1002/pssb.200490011.
21. Hodak, M.; Girifalco, L.A. Systems of C60 molecules inside (10,10) and (15,15) nanotube: A Monte Carlo study. *Phys. Rev. B* **2003**, *68*, 085405, doi:10.1103/PhysRevB.68.085405.
22. Hodak, M.; Girifalco, L.A. Ordered phases of fullerene molecules formed inside carbon nanotubes. *Phys. Rev. B* **2003**, *67*, 075419, doi:10.1103/PhysRevB.67.075419.
23. Chadli, H.; Rahmani, A.; Sbail, K.; Hermet, P.; Rols, S.; Sauvajol, J.-L. Calculation of Raman-active modes in linear and zigzag phases of fullerene peapods. *Phys. Rev. B* **2006**, *74*, 205412–205419, doi:10.1103/PhysRevB.74.205412.
24. Chadli, H.; Rahmani, A.; Sbail, K.; Sauvajol, J.-L. Raman active modes in carbon peapods. *Physica A* **2005**, *358*, 226–236, doi:10.1016/j.physa.2005.06.025.
25. Barajas-Barraza, R.E.; Guirado-Lopez, R.A. Clustering of H₂ molecules encapsulated in fullerene structures. *Phys. Rev. B* **2002**, *66*, 155426–155437, doi:10.1103/PhysRevB.66.155426.
26. Guan, L.; Li, H.; Shi, Z.; You, L.; Gu, Z. Standing or lying C70s encapsulated in carbon nanotubes with different diameters. *Solid State Commun.* **2005**, *133*, 333–337, doi.org/10.1016/j.ssc.2004.11.008.
27. Fergani, F.; Chadli, H.; Belhboub, A.; Hermet, P.; Rahmani, A. Theoretical Study of the Raman Spectra of C70 Fullerene Carbon Peapods. *J. Phys. Chem. C* **2015**, *119*, 5679–5686, doi:10.1021/jp511969t.
28. Fergani, F.; Abdelkader, S.A.A.; Chadli, H.; Fakrach, B.; Rahmani, A.H.; Hermet, P.; Rahmani, A. C60 filling rate in carbon peapods: A nonresonant raman spectra analysis. *Hindawi J. Nanomater.* **2017**, *2017*, 9248153–9248159, doi:10.1155/2017/9248153.
29. Saito, R.; Fujita, M.; Dresselhaus, G.; Dresselhaus, M.S. Electronic structure of graphene tubules based on C60. *Phys. Rev. B* **1992**, *46*, 1804–1811, doi:10.1103/PhysRevB.46.1804.
30. Hamada, N.; Sawada, S.I.; Oshiyama, A. New one-dimensional conductors: Graphitic microtubules. *Phys. Rev. Lett.* **1992**, *68*, 1579–1581, doi:10.1103/PhysRevLett.68.1579.
31. Darkrim, F. Levesque, Monte Carlo simulations of hydrogen adsorption in single-walled carbon nanotubes. *J. Chem. Phys.* **1998**, *109*, 4981, doi:10.1063/1.477109.
32. Fakrach, B.; Rahmani, A.; Chadli, H.; Sbail, K.; Bentaleb, M.; Bantignies, J.-L.; Sauvajol, J.-L. Infrared spectrum of single-walled boron nitride nanotubes. *Phys. Rev. B* **2012**, *85*, 115437–115446, doi:10.1103/PhysRevB.85.115437.
33. Jishi, R.A.; Mirie, R.M.; Dresselhaus, M.S. Force-constant model for the vibrational modes in C60. *Phys. Rev. B* **1992**, *45*, 13685–13689, doi:10.1103/PhysRevB.45.13685.
34. Soler, J.M.; Artacho, E.; Gale, J.D.; García, A.; Junquera, J.; Ordejon, P.; Sanchez-Portal, J. The SIESTA method for ab initio order-N materials simulation. *Phys. Condens. Matter* **2002**, *14*, 2745–2779, doi:10.1088/0953-8984/14/11/302.
35. Guha, S.; Menendez, J.; Page, J.B.; Adams, G.B. Empirical bond polarizability model for fullerenes. *Phys. Rev. B* **1996**, *53*, 13106–13114, doi:10.1103/PhysRevB.53.13106.
36. Benoit, C.; Royer, E.; Poussiguet, G. The spectral moments method. *J. Phys. Condens. Matter* **1992**, *4*, 3125–3131, doi:10.1088/0953-8984/4/12/010.
37. Rahmani, A.; Benoit, C.; Poussiguet, G. Vibrational properties of random percolating networks. *J. Phys. Condens. Matter* **1993**, *5*, 7941.
38. Chadli, H.; Rahmani, A.; Sauvajol, J.-L. Raman spectra of C60 dimer and C60 polymer confined inside a (10,10) single-walled carbon nanotube. *J. Phys. Condens. Matter* **2010**, *22*, 145303–145312, doi:10.1088/0953-8984/22/14/145303.
39. Chadli, H.; Fergani, F.; Bentaleb, M.; Fakrach, B.; Sbail, K.; Rahmani, A.; Bantignies, J.-L.; Sauvajol, J.-L. Influence of packing on the vibrations of homogeneous bundles of C60 peapods. *Physica E* **2015**, *71*, 31–38, doi:10.1016/j.physe.2015.03.018.

40. Bradley, C.J.; Cracknell, A.P. *The Mathematical Theory of Symmetry in Solids: Representation Theory for Point Groups and Space Groups*; Clarendon Press: Oxford, UK, 1972; ISBN-13: 978-0199582587.
41. Golberg, D.; Bando, Y.; Kurashima, K.; Soto, T. Synthesis and characterization of ropes made of BN multiwalled nanotubes. *Scr. Mater.* **2001**, *44*, 1561–1565, doi:10.1016/S1359-6462(01)00724-2.
42. Lin, F.H.; Hsu, C.K.; Tang, T.P.; Kang, P.L.; Yang, F.F. Thermal-heating CVD synthesis of BN nanotubes from trimethyl borate and nitrogen gas. *Mater. Chem. Phys.* **2008**, *107*, 115–121, doi:10.1016/j.matchemphys.2007.06.053.
43. Lee, C.H.; Wang, J.; Kayatsha, V.K.; Huang, J.Y.; Yap, Y.K. Junctions between a boron nitridenatube and a boron nitride sheet. *Nanotechnology* **2008**, *19*, 455605–455616, doi:10.1088/0957-4484/19/7/075704.
44. Lim, S.H.; Luo, J.; Wei, J.; Lin, J. Synthesis of boron nitride nanotubes and its hydrogen uptake. *Catal. Today* **2007**, *120*, 346–350, doi:10.1016/j.cattod.2006.09.016.
45. Smith, M.W.; Jordan, K.C.; Park, C.; Kim, J.W.; Lillehei, P.T.; Crooks, R.; Harrison, J.S. Very long single and few-walled boron nitride nanotubes via the pressurized vapor/condenser method. *Nanotechnology* **2009**, *20*, 505604–505609, doi:10.1088/0957-4484/20/50/505604.
46. Zhang, Z.; Guo, W.; Dai, Y. Stability and electronic properties of small boron nitride nanotubes. *J. Appl. Phys.* **2009**, *105*, 084312–084319, doi:10.1063/1.3115446.
47. Fakrach, B.; Rahmani, A.; Chadli, H.; Sbai, K.; Sauvajol, J.L. Raman spectrum of single-walled boron nitride nanotube. *Physica E* **2009**, *41*, 1800–1805, doi:10.1016/j.physe.2009.07.002.
48. Popov, V.N. Lattice dynamics of single-walled boron nitride nanotubes. *Phys. Rev. B* **2003**, *67*, 085408–085413, doi:10.1103/PhysRevB.67.085408.
49. Wirtz, L.; Rubio, A.; de la Concha, R.A.; Loiseau, A. Ab initio calculations of the lattice dynamics of boron nitride nanotubes. *Phys. Rev. B* **2003**, *68*, 045425–045437, doi:10.1103/PhysRevB.68.045425.
50. Akdim, R.; Pachter, R.; Xiaofeng, D.; Adams, W.W. Comparative theoretical study of single-wall carbon and boron-nitride nanotubes. *Phys. Rev. B* **2003**, *67*, 245404–245411, doi:10.1103/PhysRevB.67.245404.
51. Kataura, H.; Kumazawa, Y.; Maniwa, Y.; Umez, I.; Suzuki, S.; Ohtsuka, Y.; Achiba, Y. High-Yield Fullerene Encapsulation in Single-Wall Carbon Nanotubes. *Synth. Metals* **2001**, *121*, 1195–1196, doi:10.1016/S0379-6779(00)00707-4.
52. Chorro, M.; Delhey, A.; No, L.; Monthieux, M.; Launois, P. Orientation of C₇₀ molecules in peapods as a function of the nanotube diameter. *Phys. Rev. B* **2007**, *75*, 035416, doi:10.1103/PhysRevB.75.035416.
53. Liu, X.; Pichler, T.; Knupfer, M.; Golden, M.S.; Fink, J.; Kataura, H.; Achiba, Y.; Hirahara, K.; Iijima, S. Filling factors, structural, and electronic properties of C₆₀ molecules in single-wall carbon nanotubes. *Phys. Rev. B* **2002**, *65*, 045419–045424, doi:10.1103/PhysRevB.65.045419.
54. Bandow, S.; Takizawa, M.; Kato, H.; Okazaki, T.; Shinohara, H.; Iijima, S. Smallest limit of tube diameters for encasing of particular fullerenes determined by radial breathing mode raman scattering. *Chem. Phys. Lett.* **2001**, *347*, 23–28, doi:10.1016/S0009-2614(01)01020-X.

